Article:
Stone, D, Blitz, M, Ingham, T et al. (2016) An instrument to measure fast gas phase radical kinetics at hight temperatures and pressures. Review of Scientific Instruments, 87. 054102. ISSN: 0034-6748

https://doi.org/10.1063/1.4950906

An instrument to measure fast gas phase radical kinetics at high temperatures and pressures

Daniel Stone,[1] Mark Blitz,[1,2] Trevor Ingham,[1,2] Lavinia Onel,[1] Diogo J. Medeiros[1] and Paul W. Seakins[1,2]

[1] School of Chemistry, University of Leeds, Leeds, UK

[2] National Centre for Atmospheric Science, University of Leeds, Leeds, UK

Abstract

Fast radical reactions are central to the chemistry of planetary atmospheres and combustion systems. Laser-induced fluorescence is a highly sensitive and selective technique that can be used to monitor a number of radical species in kinetics experiments, but is typically limited to low pressure systems owing to quenching of fluorescent states at higher pressures. The design and characterisation of an instrument is reported using laser-induced fluorescence detection to monitor fast radical kinetics (up to 25,000 s^{-1}) at high temperatures and pressures by sampling from a high pressure reaction region to a low pressure detection region. Kinetics have been characterised at temperatures reaching 740 K and pressures up to 2 atm, with expected maximum operational conditions of up to ~ 900 K and ~ 5 atm. The distance between the point of sampling from the high pressure region and the point of probing within the low pressure region is critical to the measurement of fast kinetics. The instrumentation described in this work can be applied to the measurement of kinetics relevant to atmospheric and combustion chemistry.

Introduction

The kinetics of gas phase reactions involving free radicals are central to the chemistry of planetary atmospheres (1), interstellar space (2,3) and combustion systems (4). A variety of experimental approaches exist for the extraction of rate coefficients; for radical reactions, real-time measurements monitoring the removal of reagents or generation of products following the production of radicals by laser flash photolysis (LFP) is a successful approach (5). Laser-induced fluorescence (LIF) spectroscopy is commonly employed in flash photolysis experiments to monitor changes in radical concentrations throughout the course of a reaction in real-time, thus enabling determination of kinetic parameters. LIF is a highly sensitive and selective technique, with the sensitivity to measure OH radical concentrations in the atmosphere at concentrations of less than 10^6 cm^{-3} (6) and the selectivity to distinguish between isotopic species such as ^{16}OH and ^{18}OH (7). The nature of LFP-LIF, where the reaction is monitored only where the photolysis and probe lasers intersect, significantly reduces the potential for the influence of heterogeneous chemistry compared to flow methods. However, LIF spectroscopy is typically limited to low pressure regimes (typically < 0.5 atm) owing to collisional quenching of fluorescent states at higher pressures. Whilst many bimolecular rate coefficients are pressure independent, and hence results determined at low pressures can be used in chemical models (e.g. combustion simulations) at higher pressures, association and dissociation reactions are pressure dependent (8). Although it is sometimes possible to determine the high pressure limiting rate using isotopic (9) or proxy (10) methods, determination of rate coefficients over a wide range of temperature and pressure is important to verify theories of reactions (11) and provide kinetic input into models. Pressures in the 1 – 10 atm range are particularly relevant in elucidating autoignition processes (4,12), a subject of topical interest due to the role of autoignition in homogenous charge compression ignition (HCCI) and related engines (13,14).

Saturated laser-induced fluorescence (SLIF) spectroscopy has been successfully used to minimise the influence of collisional quenching on observed fluorescence signals at high pressures (15-18), and thus to enable determination reaction kinetics of reactive species at high pressures (up to 150 bar in He (15)). However, the technique requires sufficiently strong laser powers to ensure stimulated emission dominates over spontaneous emission and collisional quenching and can be affected by non-uniform saturation (15). In

addition, consideration of rotational energy transfer (RET) schemes are required which can complicate data analysis (15-17).

Absorption methods do not suffer from quenching and have the added advantage of providing absolute measurements if cross-sections are known. However, simple absorption methods are significantly less sensitive than LIF, although modulation methods can enhance sensitivity (19). Cavity ring down spectroscopy (CRDS) generally provides a significant enhancement in sensitivity (20-22), but as with other absorption techniques there are practical issues in maintaining uniform temperatures over the absorption region, determining the region of overlap with photolysis, avoiding surface effects and additionally keeping cavity mirrors aligned over wide pressure and temperature ranges. Thus, whilst other detection methods exist (and indeed, using a variety of methods is important to identify systematic errors), LIF has significant advantages in sensitivity, selectivity and minimising heterogeneous interferences.

In this work, we describe the use of LIF at low pressures (~ 1 Torr) in the Fluorescence Assay by Gas Expansion (FAGE) technique (23) to determine reaction kinetics of reactive species at higher pressures (> 1 atm). The FAGE technique is used by several groups worldwide (6,24-31) to measure OH radical concentrations in the atmosphere, and relies on sampling gas from a region of high pressure through a pinhole nozzle to a region of low pressure, resulting in a supersonic expansion to form a free jet. Expansion of the gas significantly reduces the rate of collisional quenching of fluorescent states, thus permitting LIF spectroscopy within the low pressure region.

Field instruments to measure the total loss rate of OH in the atmosphere (k'_{OH}, the OH reactivity) are currently in operation which use LFP in conjunction with LIF-FAGE to make real-time measurements of OH radical kinetics with ambient concentrations of trace gases at atmospheric pressure (31-38). These instruments rely on flash photolysis of O_3 (followed by the subsequent reaction of $O(^1D)$ with water vapour) to produce relatively high concentrations of OH radicals in a reaction cell containing a flow of ambient air at atmospheric pressure. The subsequent OH decay, owing to reactions with trace gases in the ambient air, is monitored by sampling from the atmospheric pressure reaction cell to the low pressure (~1-2 Torr) FAGE cell for detection by LIF.

However, ambient OH reactivity is typically low compared to reaction rates used in laboratory experiments, maximum reported values of k'_{OH} reaching ~100-120 s^{-1} even in polluted environments (37,39,40). Calibrations of OH reactivity instruments using known reactant concentrations report deviations from expected kinetics at higher reactivities, with non-exponential behaviour reported for some instruments at reactivities > 60 s^{-1} (33). Such conditions correspond to a very small dynamic range for laboratory experiments.

In this work we present the design and characterisation of an instrument to determine fast radical kinetics at high pressure and temperatures up to 740 K by coupling flash photolysis in a high pressure reaction cell to LIF in a low pressure detection cell using the FAGE technique. The use of flash photolysis to initiate the chemistry significantly lowers the potential for interference from heterogeneous chemistry. In addition to applications in combustion chemistry, we discuss the kinetic limitations of OH reactivity instruments employing similar designs, with suggestions for potential improvements. While the focus in this work is on OH kinetics, results are widely applicable to other species observable by LIF.

Experimental

Figure 1 displays a schematic of the instrument. The high pressure reaction cell consists of a stainless steel tube (304L grade) of 19 mm I.D., and length of 1 m to ensure sufficient preheating of the gas, if necessary, prior to the region near the pinhole. Gases, prepared at known concentrations and pre-mixed at known flow rates, as determined by calibrated flowmeters, are passed in to the reaction cell at one end through a T-piece which also houses a window to enable propagation of the photolysis laser beam (Lambda Physik, Compex 200 operating on either ArF at 193 nm or KrF at 248 nm, beam dimensions of 24 mm × 12 mm expanded to fill the diameter of the cell) through the cell to initiate chemistry and produce a uniform distribution of radicals throughout the cell. Precursor concentrations in the cell are maintained sufficiently low such that attenuation of the photolysis laser beam along the length of the reaction cell is negligible, leading to uniform radical concentrations along the length of the cell. The repetition rate of the photolysis

laser was varied between 1 and 10 Hz, with no impact on the observed kinetics. Gas flows in the cell are maintained under laminar conditions (Reynold's number, R_e < 2300 for laminar conditions).

At the other end of the reaction cell, the 19 mm I.D. tube is open and housed within a pressure-sealed chamber (70 mm I.D. and 200 mm in length) which couples the reaction cell to the low pressure FAGE detection cell. The open end of the reaction cell is 5 mm from the 0.5 mm pinhole nozzle which is mounted on a flat plate and enables sampling of the gas from the high pressure reaction cell into the detection cell. The flow rate of gas through the detection cell is ~ 1.2 slm (for a detection cell pressure of ~ 1 Torr), with any excess gas in the reaction cell passed out through the pressure-sealed chamber, which is connected to a rotary pump (Edwards 210 ED660). Control of the total pressure within the reaction cell is achieved by throttling the exit valve to the pump.

The temperature of the gas in the reaction cell is controlled by varying the voltage applied to a heating coil (Watlow, WATROD tubular heater) surrounding the reaction cell within the pressure-sealed chamber. Pre-heating of the gas to achieve a longer residence time in the heated region can be achieved using a ceramic heater (Watlow, ceramic fiber heater, VS102A18S) situated around the reaction cell prior to the heating coil within the pressure-sealed chamber. Three K-type thermocouples (Omega) are situated along the length of the heated region of the reaction cell to monitor the temperature.

Pressure in the detection cell is maintained at ~ 1 Torr by a rotary pump (Edwards 210 ED660) backed supercharger pump (EUROSERV). OH radicals in the gas flow are monitored by off-resonance laser-induced fluorescence following excitation at 282 nm ($A^2\Sigma$ (v'=1) ← $X^2\Pi$ (v''=0), $Q_1(1)$), generated using the 532 nm output of an Nd:YAG (Spectron Laser Systems) to pump a dye laser (Spectron Laser Systems) operating on Rhodamine-6-G dye. While 308 nm laser light offers the potential for higher sensitivity (41,42), temporal gating would be required to discriminate the fluorescence emission from scattered laser light. The 282 nm probe laser beam is passed through the detection cell perpendicular to the direction of gas flow at a variable distance (between 5 and 200 mm) from the sampling point of the gas from the reaction cell (i.e. from the position of the pinhole). The off-resonant OH fluorescence at ~308 nm is passed through an interference filter (Barr Associates, 308 ± 5 nm) and detected by a channel photomultiplier (CPM, Perkin-Elmer C1943P) mounted perpendicular to the plane of the gas flow and probe laser beam.

The time delay between photolysis and probe laser pulses is controlled by a digital delay generator (BNC DG535) and varied to enable monitoring of the OH profile as a function of time following photolysis of the gas mixture. Kinetic traces typically consist of 200 data points, with each data point typically averaged 5-10 times. OH signals are monitored before, during and after the photolysis laser pulse at several known reactant concentrations. The pseudo-first-order rate coefficient (k', where $k' = k_{OH+X}[X]$) is determined by fitting an exponential decay to the observed OH signal. The bimolecular rate coefficient (i.e. k_{OH+X}) is obtained from the gradient of the bimolecular plot (i.e. the plot of the pseudo-first-order rate coefficient against [X], the known concentration of reactant X).

Instrument characterisation at room temperature

Initial experiments to characterise the instrument and optimise experimental parameters were performed at a temperature of 298 K, total pressure of 1000 Torr, and a total flow rate of 18 slm to measure the well-known kinetics of OH + CH_3OCH_3 (dimethyl ether, DME) (18,43) by flash photolysis of $O_3/H_2O/DME/O_2/N_2$ gas mixtures. O_3 was generated from O_2 by a commercial ozone generator (EASELEC, Ozone Technology, ELO-3G), diluted in N_2 to ~ 1 % by volume and stored in an aluminium cylinder (Luxfer Gas Cylinders M4141) at a total pressure of ~6000 Torr. DME (Sigma-Aldrich, ≥ 99 %) was diluted to a known concentration in N_2 and also stored in an aluminium cylinder. Cylinders were stored overnight prior to use to ensure complete mixing, and were used within one week of preparation. No significant differences were observed between experiments using cylinders stored for different periods of time. Water vapour was introduced to the gas flow by passing the carrier gas (N_2) through a bubbler containing distilled water. N_2 (BOC, 99.99 %) and O_2 (BOC, 99.999 %) were used as supplied. OH radicals were produced in the reaction cell by the photolysis of O_3 (λ = 248 nm), followed by the subsequent reaction of $O(^1D)$ with water vapour (R1-R2). Concentrations of O_2 were sufficient to ensure that any $O(^3P)$ formed was rapidly converted back to O_3 (R3-R4). Initial OH radicals concentrations were ~1×10^{12} cm^{-3}, estimated from the laser fluence and ozone absorption cross-section at λ = 248 nm. DME concentrations were sufficient to ensure pseudo-first-order conditions for reaction with OH (R5). While there is the potential for some regeneration of OH through reaction of CH_3OCH_2 with O_2, the extent of this was small at the pressures used here (44).

$O_3 + h\nu\ (\lambda = 248\ nm) \rightarrow O(^1D) + O_2$ (R1)

$O(^1D) + H_2O \rightarrow 2\ OH$ (R2)

$O(^1D) + M \rightarrow O(^3P) + M$ (R3)

$O(^3P) + O_2 + M \rightarrow O_3 + M$ (R4)

$OH + CH_3OCH_3 \rightarrow CH_3OCH_2 + H_2O$ (R5)

Figures 2 and 3 show the observed temporal behaviour of OH and corresponding bimolecular plots for the reaction of OH with DME. At a probe distance (i.e. the distance from the pinhole, where gas is sampled from the high pressure reaction cell, to the probe laser, as shown in Figure 1) of 5 mm, the observed OH decay was well-described by pseudo-first-order kinetics and the bimolecular rate coefficient obtained for OH + DME, $k_{OH+DME} = (2.6 \pm 0.1) \times 10^{-12}$ cm^3 s^{-1}, is in good agreement with recent determinations of $k_{OH+DME} = (2.7 \pm 0.2) \times 10^{-12}$ cm^3 s^{-1} (18) and $k_{OH+DME} = (2.9 \pm 0.3) \times 10^{-12}$ cm^3 s^{-1} (43) and literature recommendations of $k_{OH+DME} = (2.8 \pm 0.4) \times 10^{-12}$ cm^3 s^{-1} (45) at 298 K. The signal-to-noise ratio of the OH measurements is estimated at ~50:1 (Figure 2), and can be improved through use of alternative OH radical precursors not requiring the presence of large amounts of water vapour, which efficiently quenches the OH fluorescent state. The sensitivity of the instrument described in this work is approximately a factor of ten lower than that achieved in a standard time-resolved LIF experiment conducted at pressures up to ~100 Torr ((43), for example). Although the number density of OH is reduced on expansion into the FAGE detection cell, the reduction in temperature associated with the expansion results in significantly increased population of the $X^2\Pi$ (v''=0), $Q_1(1)$ state probed in the experiment, reducing the impact of the decreased number density in the FAGE cell.

Measurements of the rate coefficients of reactions of OH with methane (CH_4) (see below and supplementary information for further information (46)) and isoprene (2-methyl-1,3-butadiene, C_5H_8) (see supplementary information for further information (46)) have also been obtained at probe distances of < 5 mm in agreement with literature values (45), with pseudo-first-order rate coefficients of up to ~25,000 s^{-1} measured in this work.

When probing the OH signal further away from the pinhole a significant rise time was noted for the OH signal (Figure 2b, Figures S1 and S3 in supplementary information (46)) and the resulting bimolecular plots (Figure 3b, Figures S2 and S4 in supplementary information (46)) produced a bimolecular rate coefficient that was approximately a factor two lower than the literature values. This is discussed further below.

Characterisation of temperature and pressure

Subsequent experiments were performed to characterise the instrument as a function of temperature. Figure 4 shows the temperature profiles along the reaction cell, measured by a K-type thermocouple (Omega) situated in the centre of the gas flow in the reaction cell at varying distances from the point at which gas is sampled. Temperature profiles were found to be constant in the region of the reaction cell immediately prior to the sampling point for at least 10 cm (the total heating region using the heating coil alone is ~ 18 cm in length). For a gas flow of ~ 5 slm, a distance of 1 cm in the reaction cell corresponds to a residence time of ~ 18 ms. Temperatures are monitored throughout experiments by three K-type thermocouples situated along the length of the heated region.

Kinetics of the reaction between OH and methane, CH_4, were obtained at various temperatures and pressures to characterise the instrument as a function of temperature and pressure. OH was generated by the photolysis of H_2O (λ = 193 nm) and detected at a probe distance of 5 mm from the sampling point in all cases. The OH + methane reaction was chosen for validation as it is well characterised (45,47), has a strong temperature dependence (hence a sensitive probe of the reaction temperature) and at low temperatures is a slow reaction ($k_{298\ K} = 6.3 \times 10^{-15}$ cm^3 s^{-1}) (45); reproducing literature rate coefficients at low temperatures therefore suggests an absence of interfering radical-radical reactions (47). Concentrations of CH_4 (BOC, 100 %, CP Grade, used as supplied) were sufficient to ensure pseudo-first-order conditions for OH + CH_4 at all temperatures. Total flow rates in the reaction cell were varied between 5 slm and 18 slm, with no significant effect on the observed kinetics.

206 Figure 5 shows the bimolecular rate coefficients (k_{OH+CH4}) determined in this work at temperatures in
207 the range 298 to 740 K and pressures up to 2 atm. Results obtained with this experimental approach are in
208 good agreement with those reported previously in the literature (48-50), and those currently recommended
209 for use in atmospheric (45) and combustion models (51).

210 The maximum temperatures and pressures reported in this work are primarily a result of current
211 safety constraints. To achieve the maximum temperature of 740 K reported in this work, the coil heater is
212 operating at ~75 % of its maximum power, with an expected maximum achievable temperature of ~ 900 K,
213 while current gas fittings and components within the system are specified to operate up to ~ 5 atm. It is thus
214 expected that higher temperatures and pressures could be readily achieved with this instrument than are
215 reported in this work.

216

217 Effects of probe distance

218 Measurements of k_{OH+DME} and k_{OH+CH4} obtained using the experimental approach described above
219 compare favourably with previous measurements for experiments conducted here using a short (≤ 5 mm)
220 probe distance (i.e. the distance from the point of sampling from the high pressure reaction cell at the pinhole
221 nozzle to the point at which the probe laser intersects the gas flow in the low pressure detection cell).
222 However, the probe distance has been shown to be critical to accurate kinetic measurements, as described
223 above and shown in Figures 2 and 3.

224 At longer probe distances (> 10 mm) and low reactant concentrations (i.e. with low pseudo-first-order
225 rate coefficients, < ~500 s^{-1}), the observed OH kinetics were broadly similar to literature values (Figure 3b,
226 reaction of OH with DME). However, as the reactant concentration was increased, significant deviations
227 from expected behaviour were observed when probing at longer distances. The observed OH decays at
228 higher reactant concentrations and longer probe distances appeared to display biexponential behaviour
229 (Figure 2b, reaction of OH with DME), with bimolecular rate coefficients obtained from these data
230 significantly lower than expected values (Figures 3b, reaction of OH with DME). In addition, OH signals
231 took significantly longer to appear than in experiments probing at a distance of 5 mm.

The differences observed between experiments probing at short distances from the sampling point and those probing at longer distances can be rationalised in terms of the behaviour of the gas sampled in to the low pressure detection region. When sampling from a high pressure region to a low pressure region, expansion of the sampled gas into the low pressure region results in the generation of a supersonic jet. Species within the jet can be characterised by low rotational temperatures, and have a narrow and well-defined velocity distribution around a relatively high mean velocity. The length of the jet can be approximated by the position of the Mach disk:

$$x_m = 0.67d\sqrt{p_0/p_b}$$

where $x_m$is the position of the Mach disk (i.e. the length of the jet), d is the diameter of the pinhole nozzle and $p_0$and $p_b$are the pressures in the high pressure region and the background pressure in the low pressure region, respectively. At the Mach disk, the supersonic jet breaks down and plug flow conditions dominate. Under plug flow conditions, species have higher rotational temperatures, the mean gas velocity is much lower, and the velocity distribution is much broader and can be described by a Maxwell-Boltzmann distribution.

Thus, when the distance between the sampling point (i.e. the position of the pinhole) and the detection point (i.e. the point at which the probe laser passes across the gas flow) is short (< 10 mm), the arrival time of species travelling from the sampling point to the detection point will be relatively short, with a relatively narrow distribution. The impact of this spread in arrival times on observed first-order kinetics has been described for experiments sampling from high pressure reaction regions to low pressure detection regions using mass spectrometry, and solutions enabling exact determinations of kinetics have been reported (52).

In contrast, when the distance between the sampling point and the detection point is longer (> ~10 mm for a transition from 760 Torr to 1 Torr for a 0.5 mm pinhole), species will be probed from the plug flow region. Subsequently, arrival times at the detection point will not only be much longer, but there will also be a much more significant spread of arrival times at the detection point from species which were sampled at the pinhole at the same time. The impact of this spread in arrival times will therefore be much greater if species are probed in the plug flow region than if species are probed within the jet. Deconvolution of kinetics from

transport within the detection region thus becomes more problematic under plug flow conditions, and it is not possible to obtain an exact solution to enable extraction of kinetic parameters.

Creasey et al.(53) demonstrated that the rotational temperature determined by LIF increases sharply at the expected location of the Mach disk. Figure 6 shows the LIF excitation spectra recorded for OH probed at 5 mm and 200 mm from the sampling point, indicating a transition from a low rotational temperature (~ 40 K when compared to simulations using LIFBASE (54)) at a probe distance of 5 mm to a much higher rotational temperature (~ 200 K) at a probe distance of 200 mm. Measurements of the OH LIF spectra in the detection region thus indicate that probing at a distance of 5 mm from the sampling point (where the observed kinetics indicate reliable measurements up to k' ~ 20,000 s^{-1}) probes species within the supersonic jet, while probing at a distance of 200 mm from the sampling point (where the observed kinetics deviate significantly from expected behaviour) probes species outside of the supersonic jet and within the plug flow regime.

Figure 7 shows the expected distributions of arrival times, and impacts on temporal profiles for identical pseudo-first-order reaction conditions, of species at probe regions of 5 mm from the sampling point (i.e. within the supersonic jet, simulated using the exact solution described by Taatjes (55)) and 200 mm from the sampling point (i.e. in the plug flow region, simulated using a Maxwell-Boltzmann distribution at the temperature indicated by the LIF spectra in the plug flow region). There is a clear difference in both the mean arrival time and the spread in arrival times between species probed at 5 mm and those probed at 200 mm (Figure 7a), leading to significant impacts on observed temporal profiles (Figures 2 and 5) and consequences for extraction of kinetic parameters.

Applications

Ambient OH reactivity

Deviations from the expected pseudo-first-order behaviour at high reactivities have been reported for a number of field instruments used to measure ambient OH reactivity using laser flash photolysis coupled to FAGE detection (LFP-FAGE), which typically probe OH at distances of 120-200 mm from the sampling point (31,33,36,38,56). For some instruments, such deviations from the expected exponential behaviour are

observed at reactivities above 60 s^{-1}, potentially leading to underestimations of ambient OH reactivity in polluted environments (33,34). The use of FP-FAGE to measure ambient OH reactivity does, however, offer advantages over other techniques to measure OH reactivity, particularly in high NO_x environments owing to the ability to produce OH in isolation from HO_2 which significantly reduces the impact of OH production from HO_2 + NO on the timescale of the experiment.

The observed deviations from expected behaviour at high ambient reactivities can be explained by the long probe distances typically employed in field instruments. Increased dynamic ranges for measurements of OH reactivity can thus be achieved by reducing the probe distance such that radicals are detected within the supersonic jet of the gas expansion.

Low temperature combustion

Real-time measurements of reactive species involved in low temperature combustion are key to the elucidation of reaction mechanisms involved in autoignition processes in homogeneous charge compression ignition (HCCI) engines (57). There is, however, a gap between techniques appropriate to measurements of oxidation processes at temperatures and pressures relevant to the atmosphere, and those appropriate to measurements of high temperature combustion processes in traditional spark ignition or diesel engines, limiting experimental capabilities in the temperature range ~500-900 K (57). The lack of appropriate experimental techniques for studies of low temperature combustion and the chemistry controlling autoignition has thus hindered the full exploitation of biofuels and novel fuels to improve fuel security and to reduce emissions of CO_2, NO_x and soot (4,57).

The instrumentation described in this work will bridge the gap between techniques currently described in the literature to enable more detailed investigations of the processes controlling autoignition and low temperature combustion in real-time. Dimethyl ether (DME) is a potentially promising biofuel (58), and several groups have recently reported measurements of key markers in the low temperature combustion of DME (43,59-64). However, the mechanism of DME combustion remains unclear, and the processes leading to radical chain branching have yet to be experimentally determined. Application of the techniques described

in this work to such systems will enable greater understanding of the gas phase radical chemistry involved in autoignition and low temperature combustion, and will be explored further in future work.

Summary

The design and characterisation of an instrument to measure fast gas phase kinetics in real-time at high temperatures and pressures by sampling from a high pressure reaction region to a low pressure detection region using the FAGE technique has been described. Radical generation in the high pressure reaction region is achieved by laser flash photolysis, thus minimising the potential for heterogeneous chemistry. We have demonstrated successful accurate measurements of kinetics over a range of temperatures and pressures. However, the distance between the sampling point and the probe region is critical for accurate measurements of reaction kinetics, with measurement accuracy requiring probing within the supersonic jet formed on sampling from the high pressure region to the low pressure region.

The experimental approach described in this work can be applied to measurements of fast gas phase kinetics relevant to atmospheric and combustion chemistry, and is applicable to any species exhibiting laser-induced fluorescence.

Acknowledgements

The authors are grateful to the Engineering and Physical Sciences Research Council (EPSRC, grant reference EP/J010871/1), the Natural Environment Research Council (NERC, grant reference NE/L010798/1), the National Centre for Atmospheric Science (NCAS), and the Brazilian National Council for Scientific and Technological Development (CNPq, grant reference 206527/2014-4) for funding.

Figures

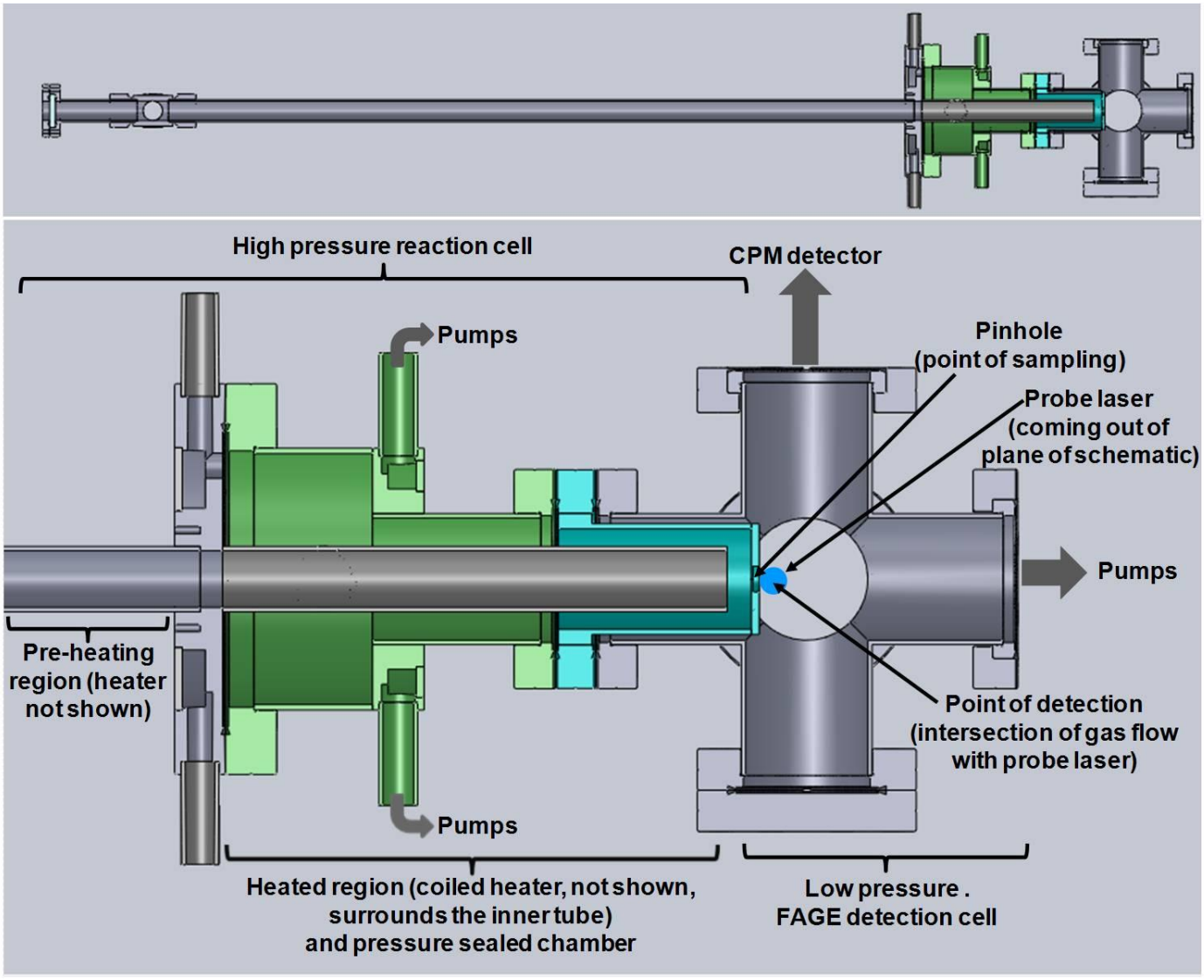

Figure 1: Schematic of the instrument. Upper panel shows the full instrument, with the lower panel displaying the region connecting the high pressure reaction cell and the low pressure detection cell in detail. The pinhole is incorporated within the section shown in blue, and this section is readily interchangeable if a change in pinhole diameter is required.

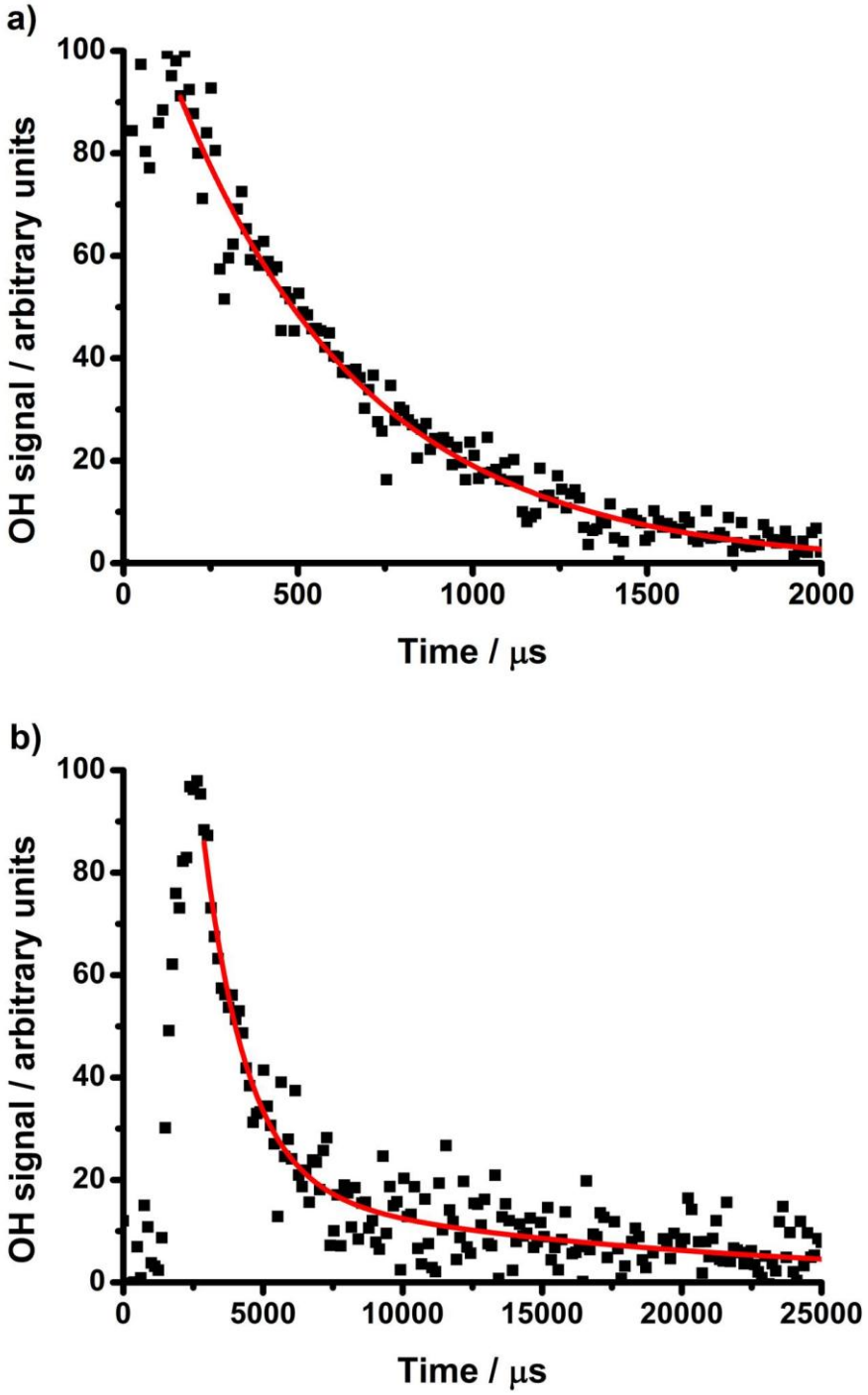

Figure 2: Temporal behaviour of OH signals for reaction of OH + CH_3OCH_3 (dimethyl ether, DME) at probe distances of a) 5 mm and b) 200 mm from the sampling point. For both plots, the reaction cell was at 298 K, 1000 Torr and the detection cell at 0.8 Torr. Fits to the data are shown in red. Data collected at a probe distance of 5 mm (panel a, [DME] = 8.3×10^{14} cm^{-3}) were fitted to a single exponential decay ($k`_{obs}$ = (1850 ± 58) $s^{-1}$), while those collected at a probe distance of 200 mm (panel b, [DME] = $3.6 \times 10^{14}$ $cm^{-3}$) were fitted to a biexponential decay ($k`_{obs,fast}$ = (644 ± 74) s^{-1}; $k`_{obs,slow}$ = (64 ± 14) s^{-1}), with only the fast component of the decay observed to display any dependence on [DME] and used in the bimolecular plots in Figure 3. Additional kinetic results obtained for OH + CH_4 at probe distances of < 5 mm and 50 mm, and for OH + C_5H_8 at a probe distance < 5 mm, are shown in the supplementary information.

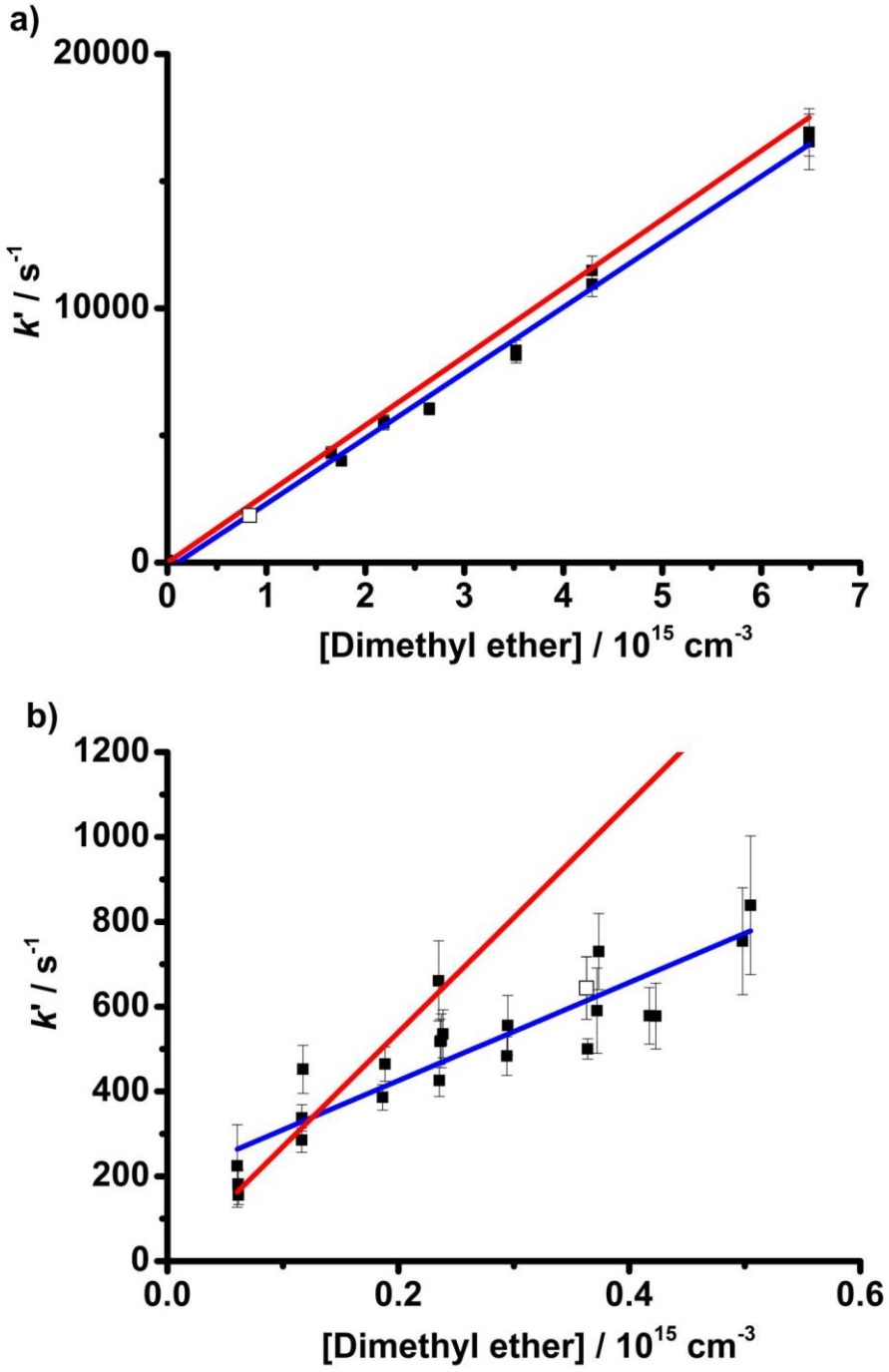

Figure 3: Bimolecular plots of observed OH decay kinetics at 298 K and 1000 Torr, with the detection cell at a pressure of 0.8 Torr, for sampling distances of a) 5 mm and b) 200 mm for reactions of OH with CH_3OCH_3 (dimethyl ether, DME). Best fit lines are shown in blue; (k = (2.6 ± 0.2) × 10^{-12} cm^3 s^{-1} when probing at 5 mm from the sampling point (panel a, analysed using a single exponential decay); k = (1.2 ± 0.2) × 10^{-12} cm^3 s^{-1} when probing at 200 mm from the sampling point (panel b, analysed using a biexponential decay)). The data points shown by the open symbols correspond to the kinetic traces shown in Figure 2. Literature recommendations shown in red (k = 2.8 × 10^{-12} cm^3 s^{-1}) (45). Note that at longer probe distances (200 mm in panel b) and low reactant concentrations, the observed OH kinetics are similar to those expected from literature values, with higher reactant concentrations leading to deviation from expected kinetics. Additional kinetic results obtained for OH + CH_4 at probe distances of < 5 mm and 50 mm, and for OH + C_5H_8 at a probe distance < 5 mm, are shown in the supplementary information.

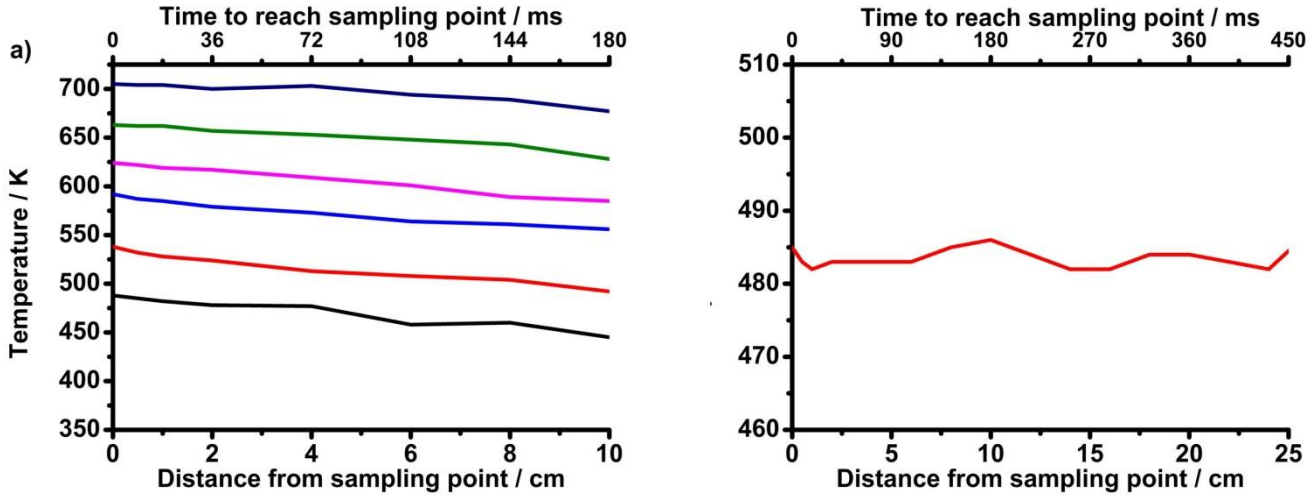

Figure 4: Temperature profiles along the length of the high pressure reaction cell (measured from the sampling point, such that the pinhole nozzle is at 0 cm). Temperatures were measured in the centre of the gas flow for flow rates of ~5 slm, corresponding to a residence time of ~ 18 ms in each 1 cm length of the reaction cell (times taken to reach the sampling point from the corresponding distance at a flow rate of 5 slm are shown in the upper *x*-axes). Pressures in the reaction cell were maintained at 1000 Torr. Panel (a) shows the temperature profiles obtained using the single heating coil only (18 cm in total length, of which only the section with stable temperature profile is shown); panel (b) shows an example temperature profile obtained using the ceramic pre-heater in addition to the coil heater.

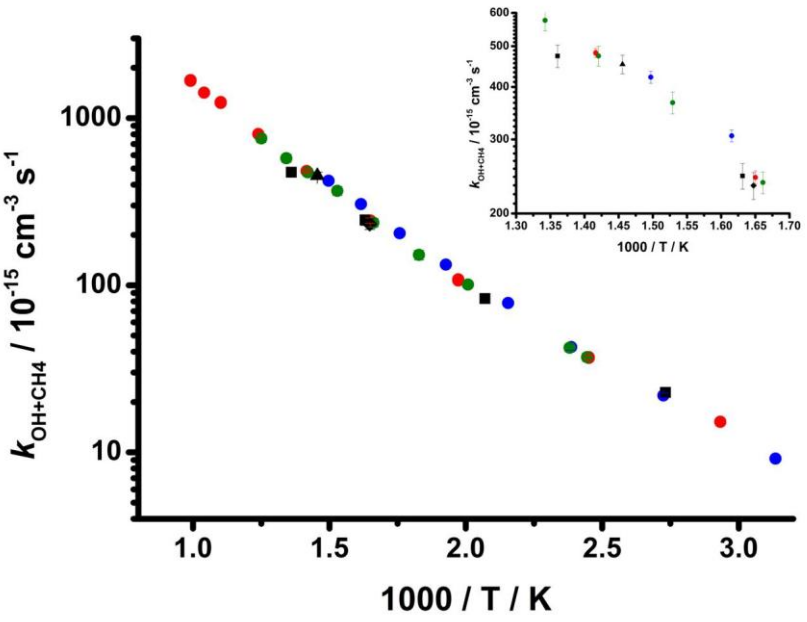

Figure 5: Bimolecular rate coefficients obtained for the reaction of OH with CH_4 as a function of temperature. Data obtained in this work are shown in the black points (squares represent data in 2 atm of N_2; diamonds represent data in 2 atm of Ar; triangles represent data in 1 atm of N_2). Previous measurements are shown for Bonard et al. (48) (blue circles), Bryukov et al. (49) (red circles) and Dunlop and Tully (50) (green circles). Errors are 2σ (although masked by the data points on the scale). The inset shows an expanded region to that the data can be seen in greater detail.

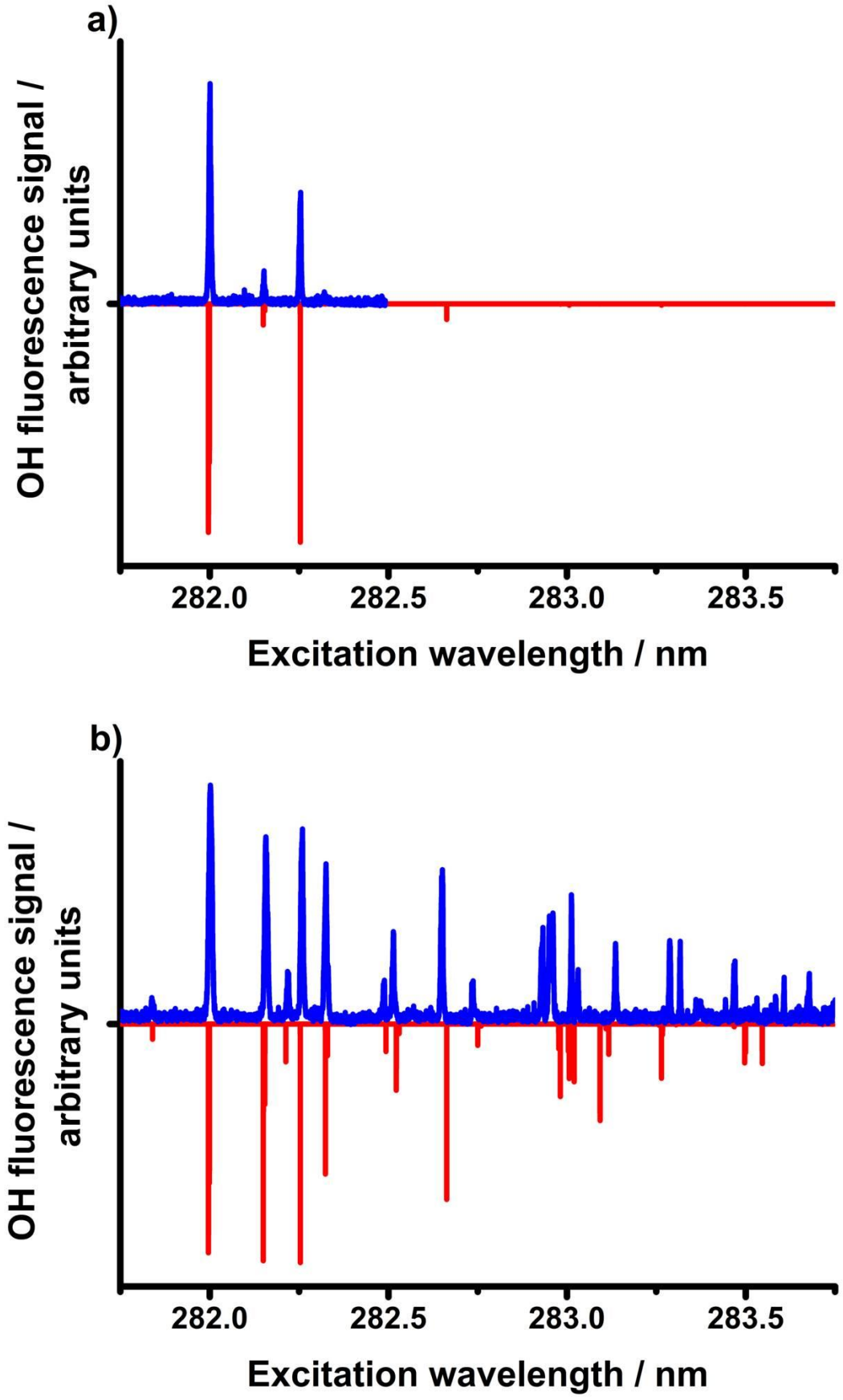

Figure 6: LIF excitation spectra for OH at sampling distances of a) 5 mm and b) 200 mm. Observed spectra are shown in blue (positive values), with LIFBASE simulations shown in red (negative values) for rotational temperatures of a) 40 K and b) 200 K. There is a sharp change in the observed spectrum at the expected location of the Mach disk (~ 12 mm in these experiments).

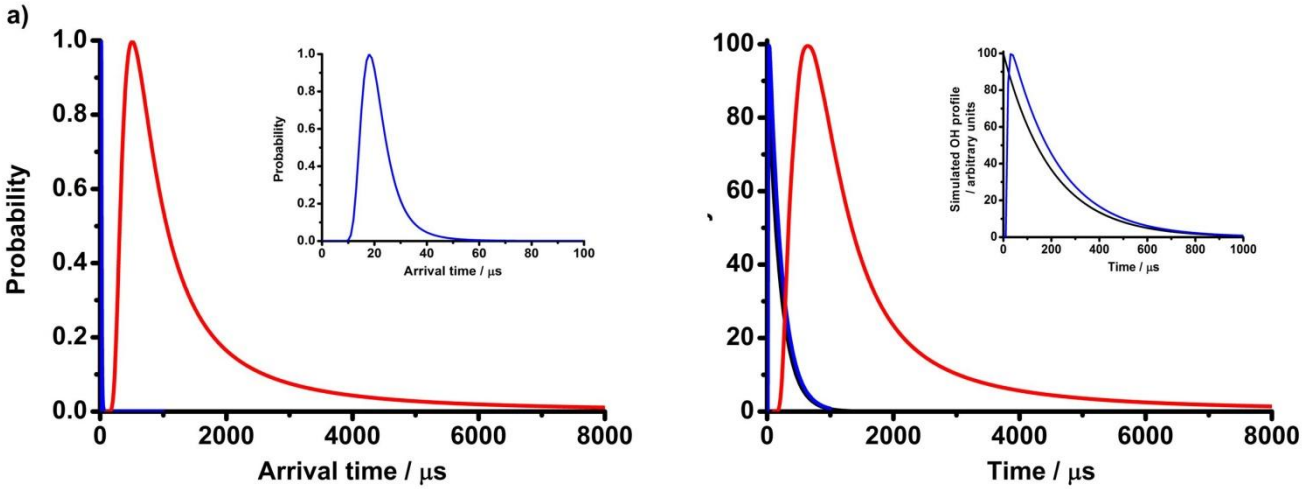

Figure 7: Simulations showing impacts of velocity distributions at probe regions of 5 mm (blue; shown more clearly in the inset plots) and 200 mm (red) on a) the normalised probabilities of arrival times at the probe region (i.e. for species leaving the sampling point at $t = 0$) and b) the apparent OH signal at the probe region for identical pseudo-first-order reaction conditions ($k` = 5000\ s^{-1}$, shown by the black line for a simulation not including any transport). Note that Creasey et al. (53), using a combination of experimental data and computational fluid dynamics calculations, demonstrated that the mean bulk gas velocity in the plug flow region was ~ 65 m s^{-1}. The impact of this slow mean bulk gas flow in our experiments is apparent from the difference in the arrival times simulated here to those observed experimentally (Figure 2b), but has not been included in these simulations since it is not possible to determine the mean bulk velocity in the plug flow region for our experimental configuration *a priori* with any certainty.

References

(1) M. A. Blitz, P. W. Seakins, Chemical Society Reviews **41**, 6318 (2012).

(2) A. Canosa, F. Goulay, I.R. Sims, B.R. Rowe, in: I.W.M. Smith (Ed.), Low Temperatures and Cold Molecules, World Scientific, Singapore, 55 (2008).

(3) I.W.M. Smith, in: S.M. Faber, E. VanDishoeck (Eds.), Annual Review of Astronomy and Astrophysics **49**, Annual Reviews, 29 (2011).

(4) J. Zador, C.A. Taatjes, R.X. Fernandes, Progress in Energy and Combustion Science **37**, 371 (2011).

(5) P.W. Seakins, Annual Reports on the Progress of Chemistry, Section C: Physical Chemistry **103** (2007).

(6) D.E. Heard, M.J. Pilling, Chemical Reviews **103**, 5163 (2003).

(7) L. D'Ottone, D. Bauer, P. Campuzano-Jost, M. Fardy, A.J. Hynes, Faraday Discussions **130**, 111 (2005).

(8) K.A. Holbrook, M.J. Pilling, S.H. Robertson, Unimolecular Reactions, Wiley, Chichester, 1996.

(9) P.W. Seakins, S.H. Robertson, M.J. Pilling, D.M. Wardlaw, F.L. Nesbitt, R.P. Thorn, W.A. Payne, L.J. Stief, Journal of Physical Chemistry **101**, 9974 (1997).

(10) I.W.M. Smith, Journal of the Chemical Society-Faraday Transactions **93**, 3741 (1997).

(11) M.A. Blitz, N.J.B. Green, R.J. Shannon, M.J. Pilling, P.W. Seakins, C.M. Western, S.H. Robertson, Journal of Physical Chemistry A **119**, 7668 (2015).

(12) M.J. Pilling, S.H. Robertson, P.W. Seakins, Journal of the Chemical Society-Faraday Transactions **91**, 4179 (1995).

(13) C.K. Westbrook, W.J. Pitz, H.J. Curran, in: H. Zhao (Ed.), HCCI and CAI engines for the automotive industry, CRC Press, Boca Raton, (2007).

(14) M.F. Yao, Z.L. Zheng, H.F. Liu, Progress in Energy and Combustion Science **35**, 398 (2009).

(15) R. Forster, M. Frost, D. Fulle, H.F. Hamann, H. Hippler, A. Schlepegrell, J. Troe, Journal of Chemical Physics **103**, 2949 (1995).

(16) R.V. Ravikrishna, C.S. Cooper, N.M. Laurendeau, Combustion and Flame **117**, 810 (1999).

(17) K. Kohse-Hoinghaus, W. Perc, T. Just, Berichte Der Bunsen-Gesellschaft-Physical Chemistry Chemical Physics **87**, 1052 (1983).

(18) C. Bansch, J. Kiecherer, M. Szori, M. Olzmann, Journal of Physical Chemistry A **117**, 8343 (2013).

(19) A.M. Knepp, G. Meloni, L.E. Jusinski, C.A. Taatjes, C. Cavallotti, S.J. Klippenstein, Physical Chemistry Chemical Physics **9**, 4315 (2007).

(20) A. Bossolasco, E.P. Farago, C. Schoemaecker, C. Fittschen, Chemical Physics Letters, **593**, 7 (2014).

(21) A.E. Parker, C. Jain, C. Schoemaecker, P. Szriftgiser, O. Votava, C. Fittschen, Applied Physics B-Lasers and Optics **103**, 725 (2011).

(22) M.D. Wheeler, S.M. Newman, A.J. Orr-Ewing, M.N.R. Ashfold, Journal of the Chemical Society-Faraday Transactions **94**, 337 (1998).

(23) T .M. Hard, R.J. O'Brien, C.Y. Chan, A.A. Mehrabzadeh, Environmental Science & Technology **18**, 768 (1984).

(24) D. Stone, L.K. Whalley, D.E. Heard, Chemical Society Reviews **41**, 6348 (2012).

(25) D.J. Creasey, P.A. Halford-Maw, D.E. Heard, M.J. Pilling, B.J. Whitaker, Journal of the Chemical Society-Faraday Transactions **93**, 2907 (1997).

(26) D. Tan, I. Faloona, J.B. Simpas, W. Brune, J. Olson, J. Crawford, M. Avery, G. Sachse, S. Vay, S. Sandholm, H.W. Guan, T. Vaughn, J. Mastromarino, B. Heikes, J. Snow, J. Podolske, H. Singh, Journal of Geophysical Research-Atmospheres **106**, 32667 (2001).

(27) F. Holland, M. Hessling, A. Hofzumahaus, Journal of the Atmospheric Sciences **52**, 3393 (1995).

(28) M. Martinez, H. Harder, D. Kubistin, M. Rudolf, H. Bozem, G. Eerdekens, H. Fischer, T. Klupfel, C. Gurk, R. Konigstedt, U. Parchatka, C.L. Schiller, A. Stickler, J. Williams, J. Lelieveld, Atmospheric Chemistry and Physics **10**, 3759 (2010).

(29) S. Dusanter, D. Vimal, P.S. Stevens, Atmos. Chem. Phys. **8**, 321 (2008).

(30) Y. Kanaya, H. Akimoto, The Chemical Record **2**, 199 (2002).

(31) D. Amedro, K. Miyazaki, A. Parker, C. Schoemaecker, C. Fittschen, Journal of Environental Sciences-China **24**, 78 (2012).

(32) Y. Sadanaga, A. Yoshino, K. Shungo, K. Yoshizumi, Environmental Science & Technology **39**, 8847 (2005).

(33) S. Lou, F. Holland, F. Rohrer, K. Lu, B. Bohn, T. Brauers, C.C. Chang, H. Fuchs, R. Haseler, K. Kita, Y. Kondo, X. Li, M. Shao, L. Zeng, A. Wahner, Y. Zhang, W. Wang, A. Hofzumahaus, Atmospheric Chemistry and Physics **10**, 11243 (2010).
(34) K. Lu, F. Rohrer, F. Holland, H. Fuchs, B. Bohn, T. Brauers, C.C. Chang, R. Haeseler, M. Hu, K. Kita, Y. Kondo, X. Li, S. Lou, S. Nehr, M. Shao, L. Zeng, A. Wahner, Y. Zhang, A. Hofzumahaus, Atmos Chem Phys **12**, 1541 (2012).
(35) K.D. Lu, A. Hofzumahaus, F. Holland, B. Bohn, T. Brauers, H. Fuchs, M. Hu, R. Haseler, K. Kita, Y. Kondo, X. Li, S.R. Lou, A. Oebel, M. Shao, L.M. Zeng, A. Wahner, T. Zhu, Y.H. Zhang, F. Rohrer, Atmospheric Chemistry and Physics **13**, 1057 (2013).
(36) A.E. Parker, D. Amedro, C. Schoemaecker, C. Fittschen, Environmental Engineering and Management Journal **10**, 107 (2011).
(37) L.K. Whalley, D. Stone, R. Dunmore, J.F. Hamilton, J. Hopkins, J.D. Lee, B. Bandy, D.E. Heard, Atmospheric Chemistry and Physics **16**, 2109 (2016).
(38) D. Stone, L.K. Whalley, T. Ingham, P.M. Edwards, D. Cryer, C. Brumby, P.W. Seakins, D.E. Heard, Atmospheric Measurement Techniques Discussions, doi:10.5194/amt-2016-51, in review (2016).
(39) T.R. Shirley, W.H. Brune, X. Ren, J. Mao, R. Lesher, B. Cardenas, R. Volkamer, L.T. Molina, M.J. Molina, B. Lamb, E. Velasco, T. Jobson, M. Alexander, Atmospheric Chemistry and Physics **6**, 2753 (2006).
(40) V.G.C. Dolgorouky, R. Sarda-Esteve, V. Sinha, J. Williams, N. Marchand, S. Sauvage, L. Poulain, J. Sciare, B. Bonsang, Atmospheric Chemistry and Physics **12**, 9593 (2012).
(41) C.Y. Chan, T.M. Hard, A.A. Mehrabzadeh, L.A. George, R.J. O'Brien, Journal of Geophysical Research **95**, 18569 (1990).
(42) P.S. Stevens, J.H. Mather, W.H. Brune, Journal of Geophysical Research-Atmospheres **99**, 3543 (1994).
(43) S.A. Carr, T.J. Still, M.A. Blitz, A.J. Eskola, M.J. Pilling, P.W. Seakins, R.J. Shannon, B. Wang, S.H. Robertson, Journal of Physical Chemistry A **117**, 11142 (2013).
(44) A.J. Eskola, S.A. Carr, R.J. Shannon, B. Wang, M.A. Blitz, M.J. Pilling, P.W. Seakins, S.H. Robertson, Journal of Physical Chemistry A **118**, 6773 (2014).
(45) R. Atkinson, D.L. Baulch, R.A. Cox, J.N. Crowley, R.F. Hampson, R.G. Hynes, M.E. Jenkin, M.J. Rossi, J. Troe, Atmosperic Chemistry and Physics **6**, 3625 (2006).
(46) See supplemental information for further details of kinetic measurements of reactions of OH with methane and isoprene as a function of the probe distance.
(47) G.L. Vaghjiani, A.R. Ravishankara, Nature **350**, 406 (1991).
(48) A. Bonard, V. Daele, J.L. Delfau, C. Vovelle, Journal of Physical Chemistry A **106**, 4384 (2002).
(49) M.G. Bryukov, V.D. Knyazev, S.M. Lomnicki, C.A. McFerrin, B. Dellinger, Journal of Physical Chemistry A **108**, 10464 (2004).
(50) J.R. Dunlop, F.P. Tully, Journal of Physical Chemistry **97**, 11148 (1993).
(51) D.L. Baulch, C.T. Bowman, C.J. Cobos, R.A. Cox, T. Just, J.A. Kerr, M.J. Pilling, D. Stocker, J. Troe, W. Tsang, R.W. Walker, J. Warnatz, Journal of Physical and Chemical Reference Data **34**, 757 (2005).
(52) M.T. Baeza-Romero, M.A. Blitz, A. Goddard, P.W. Seakins, International Journal of Chemical Kinetics **44**, 532 (2012).
(53) D.J. Creasey, D.E. Heard, M.J. Pilling, B.J. Whitaker, M. Berzins, R. Fairlie, Applied Physics B-Lasers and Optics **65**, 375 (1997).
(54) J. Luque, D.R. Crosley, LIFBASE: Database and Spectral Simulation Program, SRI International (1995).
(55) C.A. Taatjes, International Journal of Chemical Kinetics **39**, 565 (2007).
(56) Y. Sadanaga, A. Yoshino, K. Watanabe, A. Yoshioka, Y. Wakazono, Y. Kanaya, Y. Kajii, Review of Scientific Instruments **75**, 2648 (2004).
(57) D.K. Manley, A. McIlroy, C.A. Taatjes, Physics Today **61**, 47 (2008).
(58) T.A. Semelsberger, R.L. Borup, H.L. Greene, Journal of Power Sources **156**, 497 (2006).
(59) H. Guo, W. Sun, F.M. Haas, T. Farouk, F.L. Dryer, Y. Ju, Proceedings of the Combustion Institute **34**, 573 (2013).
(60) F. Herrmann, B. Jochim, P. Oswald, L. Cai, H. Pitsch, K. Kohse-Hoeinghaus, Combustion and Flame **161**, 384 (2014).

(61) N. Kurimoto, B. Brumfield, X. Yang, T. Wada, P. Dievart, G. Wysocki, Y. Ju, Proceedings of the Combustion Institute **35**, 457 (2015).

(62) K. Moshammer, A.W. Jasper, D.M. Popolan-Vaida, A. Lucassen, P. Dievarti, H. Selim, A.J. Eskola, C.A. Taatjes, S.R. Leone, S.M. Sarathy, Y. Ju, P. Dagaut, K. Kohse-Hoeinghaus, N. Hansen, Journal of Physical Chemistry A **119**, 7361 (2015).

(63) T. Ngoc Linh Le, M. Djehiche, C.D. Jain, P. Dagaut, G. Dayma, Fuel **158**, 248 (2015).

(64) A. Rodriguez, O. Frottier, O. Herbinet, R. Fournet, R. Bounaceur, C. Fittschen, F. Battin-Leclerc, Journal of Physical Chemistry A **119**, 7905 (2015).